Aging Cell (2011) **10,** pp172–183 Doi: 10.1111/j.1474-9726.2010.00652.x

Iron handling in hippocampal neurons: activity-dependent iron entry and mitochondria-mediated neurotoxicity

Ilaria Pelizzoni,[1,2] Romina Macco,[1,3] Marco Francesco Morini,[1]* Daniele Zacchetti,[1,2] Fabio Grohovaz[1,2,3] and Franca Codazzi[1,2]

[1]Cellular Neurophysiology Unit, Division of Neuroscience, San Raffaele Scientific Institute, via Olgettina 58, I-20132 Milano, Italy
[2]Italian Institute of Technology (IIT), Research Unit of Molecular Neuroscience, via Olgettina 58, I-20132 Milano, Italy
[3]San Raffaele University, via Olgettina 58, I-20132 Milano, Italy

Summary

The characterization of iron handling in neurons is still lacking, with contradictory and incomplete results. In particular, the relevance of non-transferrin-bound iron (NTBI), under physiologic conditions, during aging and in neurodegenerative disorders, is undetermined. This study investigates the mechanisms underlying NTBI entry into primary hippocampal neurons and evaluates the consequence of iron elevation on neuronal viability. Fluorescence-based single cell analysis revealed that an increase in extracellular free Fe^{2+} (the main component of NTBI pool) is sufficient to promote Fe^{2+} entry and that activation of either N-methyl-D-aspartate receptors (NMDARs) or voltage operated calcium channels (VOCCs) significantly potentiates this pathway, independently of changes in intracellular Ca^{2+} concentration ($[Ca^{2+}]_i$). The enhancement of Fe^{2+} influx was accompanied by a corresponding elevation of reactive oxygen species (ROS) production and higher susceptibility of neurons to death. Interestingly, iron vulnerability increased in aged cultures. Scavenging of mitochondrial ROS was the most powerful protective treatment against iron overload, being able to preserve the mitochondrial membrane potential and to safeguard the morphologic integrity of these organelles. Overall, we demonstrate for the first time that Fe^{2+} and Ca^{2+} compete for common routes (i.e. NMDARs and different types of VOCCs) to enter primary neurons. These iron entry pathways are not controlled by the intracellular iron level and can be harmful for neurons during aging and in conditions of elevated NTBI levels. Finally, our data draw the attention to mitochondria as a potential target for the treatment of the neurodegenerative processes induced by iron dysmetabolism.

Key words: calcium; hippocampal neurons; iron; mitochondria; neurotoxicity; oxidative stress.

Introduction

The central nervous system relies on iron availability for many essential functions but it is also highly vulnerable to iron-induced oxidative stress. Indeed, progressive accumulation of iron in a normal aging brain (Stankiewicz & Brass, 2009) or pathologic alterations of its homeostasis can be the cause or a contributory cause in the neurodegeneration processes observed in many neurologic disorders (Andersen, 2004; Madsen & Gitlin, 2007; MacKenzie *et al.*, 2008; Altamura & Muckenthaler, 2009; Benarroch, 2009; Stankiewicz & Brass, 2009). A disruption of iron handling might also play an important role in acute neuronal injury states characterized by an increase in intracellular free iron, such as cerebral ischemia (Bralet *et al.*, 1992; Lipscomb *et al.*, 1998).

The control of brain iron homeostasis is a debated issue, with open questions and controversial results (Moos & Morgan, 2004). Indeed, the mechanisms and the proteins involved in iron handling are differentially represented, not only within the various cell types, but also in different brain areas (Wu *et al.*, 2004; Zecca *et al.*, 2004).

In the brain interstitial fluids the concentration of iron exceeds the binding capacity of transferrin (Tf) (Qian & Shen, 2001; Ma *et al.*, 2009). This residual iron pool, called non-transferrin-bound iron (NTBI), is composed by free iron as well as iron bound to other proteins (e.g. lactoferrin, melanotransferrin) or loosely associated to inorganic carrier molecules (e.g. citrate, ascorbate, ATP) (Bradbury, 1997; Moos *et al.*, 2007). The uptake of NTBI is an important iron source for different cell types in the brain, but it is also a potentially hazardous factor. Little is known about the molecules involved in the mechanisms controlling NTBI uptake. Results obtained in neuronal cells suggest NTBI uptake to be mediated by divalent metal transporter 1 (DMT1) activity and controlled by $[Ca^{2+}]_i$ (Cheah *et al.*, 2006). Other experimental evidence shows, in cardiomyocytes and in neuronal cell lines, the possibility of a common entry pathway for Ca^{2+} and Fe^{2+} (Oudit *et al.*, 2003; Gaasch *et al.*, 2007a).

This work was aimed at the characterization of the NTBI influx pathways in rat hippocampal primary cultures, with specific interest to the involvement of voltage operated calcium

Correspondence
F. Grohovaz or F. Codazzi, San Raffaele Scientific Institute, via Olgettina 58, 20132 Milano, Italy. Tel.: +39 02 2643 4811; fax: +39 02 2643 4813; e-mails: grohovaz.fabio@hsr.it or codazzi.franca@hsr.it

*Present address: IFOM, FIRC Institute of Molecular Oncology, Campus IFOM-IEO, Via Adamello, 16 I-20139 Milano, Italy.

Accepted for publication *7 November 2010*

channels (VOCCs) and N-methyl-D-aspartate receptors NMDARs). We also investigated the role iron entry has on the production of reactive oxygen species (ROS). In particular, we focused on mitochondria since they are the major production site of hydrogen peroxide that, in the presence of iron, gives rise to hydroxyl radicals, largely responsible for the neurotoxic effects observed during aging and in several neurodegenerative diseases (Fariss *et al.*, 2005; Giorgio *et al.*, 2007; Galaris *et al.*, 2008).

Results

Iron entry in hippocampal neurons

The mechanisms of iron entry were investigated by videomicroscopy in rat hippocampal primary cultures (Codazzi *et al.*, 2006) where neurons were distinguished from astrocytes based on their morphologic features or on their specific response to the glutamatergic agonist N-methyl-D-aspartic acid (NMDA, added at the end of the experiments).

Iron influx in cells has long been evaluated by exploiting the capability of iron to quench the fluorescence of different dyes. Although calcein is widely considered as the main iron probe (Cabantchik *et al.*, 1996; Esposito *et al.*, 2002), fura-2 has recently been proposed for this purpose, also considering its differential sensitivity to Fe^{2+} (Kd 10^{-9}) and Fe^{3+} (Kd 10^{-6}) that allows the discrimination of the two iron forms (Kress *et al.*, 2002).

In a first set of experiments, the two dyes were concomitantly loaded and variations of fluorescence were monitored in neurons, in response to changes in intracellular Fe^{2+}. Controlled iron entry was obtained by administering increasing concentrations of extracellular Fe^{2+} in the presence of 20 μM pyrithione, an iron ionophore (Kress *et al.*, 2002). The two traces in Fig. 1A show that fura-2 is more sensitive to fluorescence quenching than calcein. Moreover, when Fe^{2+} was oxidized by administration of H_2O_2, a recovery of fura-2 fluorescence was observed, as a consequence of Fe^{3+} unbinding because of the diminished affinity. On the contrary, iron oxidation led to a variation of calcein fluorescence that was lower, and that caused further quenching (due to higher affinity of calcein for Fe^{3+} than Fe^{2+}) of the fluorescence signal, close to background values. Considering that fura-2 was more suitable to reveal small variations of intracellular Fe^{2+} concentration and reliable in monitoring iron oxidation in live cells, the dye was employed throughout our work. Moreover, the use of fura-2 allowed us to concomitantly measure the variations of $[Ca^{2+}]_i$ (excitation at 340 and 380 nm) as well as the changes in free cytosolic iron (excitation at 355 nm, the Ca^{2+}-insensitive wavelength in our optical system, see Experimental procedures) within individual cells. Changes in fura-2 fluorescence due to $[Ca^{2+}]_i$ increases did not affect the Fe^{2+}-mediated fura-2 quenching at 355 nm and *vice versa* (see as an example Fig. 6A).

When neurons were challenged by extracellular administration of 100 μM Fe^{2+} the fluorescence signal underwent a slight but continuous quenching that reached a steady state within 30 min (Fig. 1B). Administration of 100 μM salicylaldehyde isonicotinoyl hydrazone (SIH), an intracellular iron chelator (Shvartsman *et al.*, 2007), promoted a substantial recovery of fluorescence, indicating that the previous quenching was specifically due to Fe^{2+} entry. Interestingly, the quenching following exposure to Fe^{2+} was higher when neurons were previously depolarized for 30 min with 30 mM KCl or pre-treated for the same period of time with 100 μM NMDA (Fig. 1B). The potentiation of Fe^{2+} entry was observed also when KCl or NMDA were administered acutely. In this case, the first phase of quenching, after adding Fe^{2+}, was followed by a second phase due to an increase in iron entry and concomitant to the activation of either VOCCs or NMDARs (data not shown). We next explored the mechanisms responsible for the potentiation of Fe^{2+} entry upon

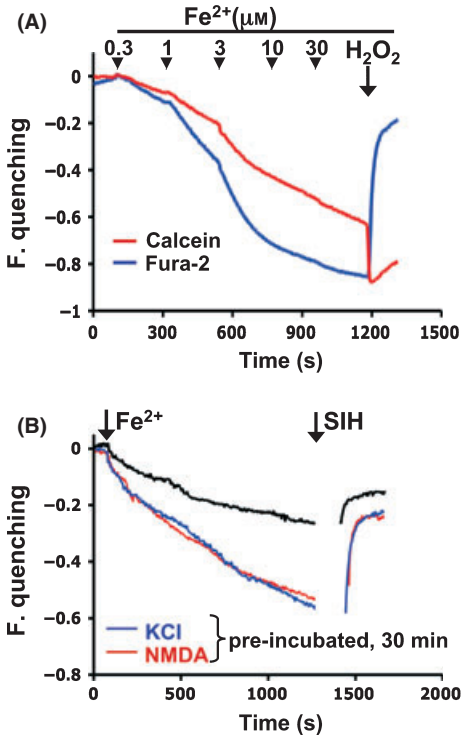

Fig. 1 Analysis of iron variations in hippocampal neurons. (A) Single cell imaging was performed on hippocampal neurons loaded with 4 μM fura-2 (355 nm excitation) and 0.25 μM calcein (488 nm excitation). To obtain a controlled entry of Fe^{2+}, neurons were exposed to an iron ionophore (20 μM pyrithione for 3 min), before adding increasing concentrations (as indicated) of ferrous-ammonium sulfate. In this and in the following figures, traces show quenching of fluorescence signals (F. quenching) as the fluorescence decrease with respect to basal values. The two traces (mean signals obtained from all the neurons present in the analyzed field) show an iron-mediated quenching which is higher for fura-2 than for calcein. Oxidation of Fe^{2+} to Fe^{3+}, mediated by 500 μM H_2O_2 promoted strong recovery of fura-2 signal, while further quenching of calcein signal. (B) Sole administration of 100 μM Fe^{2+} to fura-2-loaded hippocampal neurons promoted fluorescence quenching as a consequence of Fe^{2+} entry (black trace). Quenching was increased when neuronal cells were pre-treated for 30 min with 30 mM KCl or 100 μM N-methyl-D-aspartic acid (NMDA). A fast fluorescence recovery was observed upon administration of 100 μM salicylaldehyde isonicotinoyl hydrazone (SIH), a cell permeant iron chelator. Traces are from three representative hippocampal neurons analyzed in separate experiments.

depolarization or NMDAR stimulation. Since a recent paper (Oudit *et al.*, 2003) demonstrated an iron influx in cardiomyocytes through L-type Ca^{2+} channels, we evaluated the possible relevance of this pathway also in hippocampal neurons. Accordingly, Fe^{2+} entry was analyzed in terms of percentage of quenching at the steady state under various experimental conditions. Administration of 10 μM nimodipine, a selective L-type Ca^{2+} channel blocker, did not reduce basal Fe^{2+} influx and only partially decreased the cytosolic Fe^{2+} accumulation after depolarization (Fig. 2A). The implication of L-type Ca^{2+} channels was, on the other hand, confirmed by the effect of BAY K 8644 (10 μM), an L-VOCC agonist, that, in combination with KCl, further enhanced Fe^{2+} influx (50.5% of quenching compared to 38.5% obtained by KCl alone). When neurons were pre-treated with a mix of blockers for the VOCC family (Mix: 10 μM nimodipine for L-type, 10 μM NNC 55-0396 for T-type, and 1 μM ω-conotoxin MVIIC for N-, P-, Q-types), Fe^{2+} influx was reduced both in resting conditions and after depolarization (Fig. 2A). This result strongly suggests that Fe^{2+} can enter hippocampal neurons not only through L-VOCCs but also other types of neuronal Ca^{2+} channels.

Since a potentiation of iron entry after NMDAR stimulation was reported in a recent study (Cheah *et al.*, 2006), we investigated the Fe^{2+}-mediated fura-2 quenching after administration of two concentrations of NMDA (submaximal, 20 μM; and maximal, 100 μM) either in acute or pre-incubated for 30 min. The lower concentration was chosen to maintain a marked response while restraining short-term toxic effects. The potentiation promoted by NMDA stimulation was observed in the above conditions, and it was completely reverted by 20 μM MK-801, a non-competitive antagonist of NMDARs (Fig. 2B). Interestingly, while the mix of VOCC blockers reduced Fe^{2+} uptake at rest, a similar reduction was not observed in the presence of MK-801.

Since physiologic concentration of NTBI in the interstitium and in cerebrospinal fluids is estimated to be in the low micromolar range (from ~0.4 to 3.5 μM; Bradbury, 1997; Molina *et al.*, 1998; Mills *et al.*, 2010), we verified whether Fe^{2+} influx was appreciable also when hippocampal neurons were exposed to a range of Fe^{2+} concentrations comprised between 1 and 100 μM. The dose–response relationship showed a measurable fura-2 quenching at all concentrations considered (Fig. 2C). Furthermore, a potentiation mediated by VOCC and NMDAR stimulation was observed even at extracellular Fe^{2+} concentration as low as 1 μM (increase of quenching from 5.0 to 12.2 ± 1.06 and 12.3 ± 1.65 ,respectively; four experiments) and 5 μM (increase of quenching from 6.3 to 11.4 ± 1.36 and 11 ± 1.6, respectively; four experiments). Finally, we verified the selective permeability of VOCCs and NMDARs to Fe^{2+}. Hippocampal cultures were loaded with both fura-2 and calcein (more sensitive to Fe^{2+} and Fe^{3+}, respectively, see Fig. 1A) and exposed to 100 μM Fe^{3+} (administered as ferric ammonium citrate). We observed no changes in calcein fluorescence (not shown) and only a moderate quenching of fura-2 (Fig. 2C). This small increase in intracellular Fe^{2+} can be accounted for by the activity of ferrireductases, which are known to be expressed in the brain

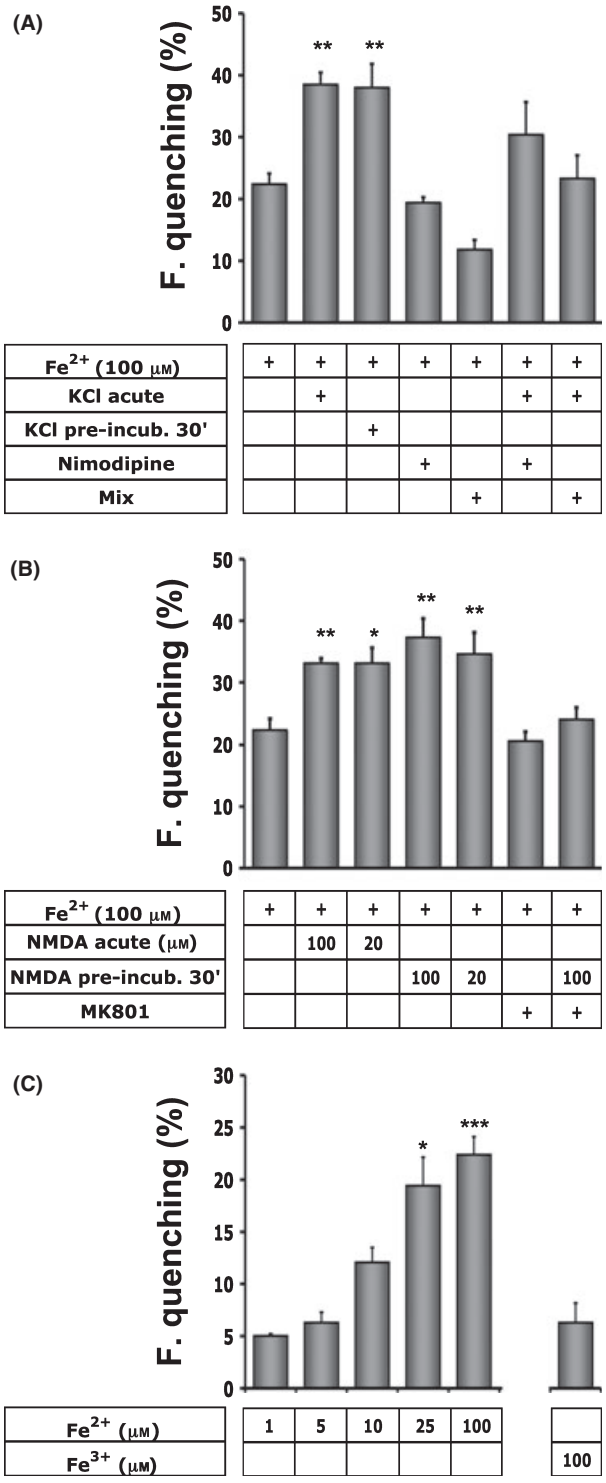

Fig. 2 Fe^{2+} entry in hippocampal neurons under different experimental conditions. The bars in the three panels represent the average (± SEM) percent quenching of fura-2 for the indicated experimental conditions. The mean value was obtained from the analysis of individual cells (panel A and B: 7–12 separate experiments for each condition; panel C: 4–5 experiments; ~8 neurons per experiment). Statistical significance was calculated using one-way ANOVA followed by Dunnett's *post hoc* test; $*P < 0.05$; $**P < 0.01$.

(Vargas *et al.*, 2003; Mills *et al.*, 2010), and by the subsequent entry through Ca^{2+} channels; in line with this hypothesis, quenching was mainly observed in neurons showing spontaneous activity, i.e. in neurons where Ca^{2+} channels have an increased open probability.

Role of Ca^{2+} on Fe^{2+} influx

These results suggest that iron influx is governed by the extent of activation of VOCCs or NMDARs but leave open the issue of whether Fe^{2+} influx is directly controlled by the channel opening or involves other pathways (such as DMT1) modulated by the Ca^{2+} influx (Cheah *et al.*, 2006). The typical protocol to investigate the effect of Ca^{2+} influx would involve the use of intra- or extra-cellular Ca^{2+} chelators, such as BAPTA (1,2-bis(o-aminophenoxy) ethane-N,N,N′,N′-tetraacetic acid) and ethylene glycol tetraacetic acid (EGTA). Unfortunately, they cannot be employed because Fe^{2+} would be chelated as well (Britigan *et al.*, 1998). Accordingly, we performed a set of experiments using a Ca^{2+}- and Mg^{2+}-free KRH where the traces of the two cations were removed by incubation with the ion exchange resin CHELEX-100 (Ca^{2+}/Mg^{2+}-free KRH, see Experimental procedures). When Fe^{2+} was administered in the presence of decreasing concentrations of extracellular Ca^{2+} (2, 0.1 mM and Ca^{2+}/Mg^{2+}-free KRH), fura-2 quenching was progressively increased suggesting a competition between Fe^{2+} and Ca^{2+} for the same entry pathways (Fig 3A). Since the strong increase in Fe^{2+} influx often induced premature neuronal death, we restricted the comparative analysis to the first 10 min. Figure 3B shows neurons at rest soaked in Ca^{2+}/Mg^{2+}-free KRH and exposed to iron load. Under these conditions, iron influx was greatly inhibited when VOCCs, but not NMDARs, were blocked, suggesting that only the former play a significant role in unstimulated neurons. On the other hand, both pathways can contribute to iron influx, as indicated by the change in the slope of quenching when either 30 mM KCl or 100 μM NMDA was administered (Fig. 3C). This effect was more evident when lower concentrations of Fe^{2+} were administered (5–20 μM; not shown). Interestingly, iron passage through both VOCCs and NMDARs was clearly reduced when Ca^{2+} was restored in the extracellular solution (Fig. 3B,D), providing further support to the idea that the two ions compete

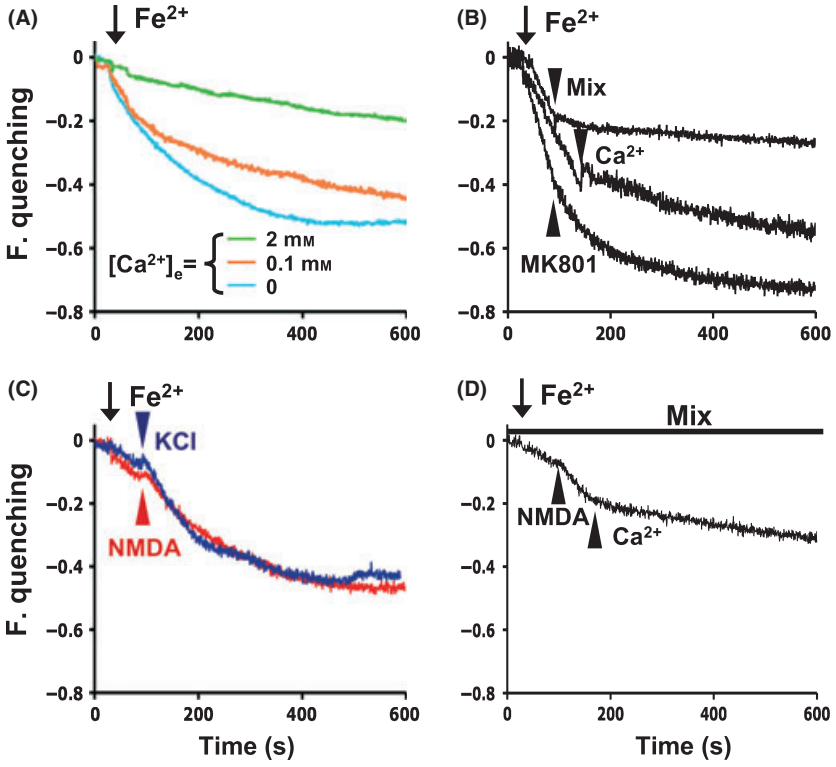

Fig. 3 Common pathways for Ca^{2+} and Fe^{2+} entry in hippocampal neurons. (A) the three traces represent fura-2 fluorescence quenching upon administration of 100 μM Fe^{2+} in the presence of the indicated concentrations of extracellular Ca^{2+}. Each trace represents an average of the neurons (n = 6–10) analyzed in 5 (2 mM Ca^{2+}), 6 (0.1 mM Ca^{2+}) and 9 [Ca^{2+}/Mg^{2+}-free Krebs Ringer Hepes (KRH)] experiments. Ca^{2+} appears to compete with Fe^{2+} for entry. (B–D) In all experiments, 100 μM Fe^{2+} was administered to unstimulated neurons exposed to Ca^{2+}/Mg^{2+}-free KRH. (B) Fe^{2+}-mediated fura-2 quenching was unaffected by 20 μM MK801, an N-methyl-D-aspartate (NMDAR) antagonist (two experiments), partially inhibited by restoring physiologic $[Ca^{2+}]_e$ (2 mM; 10 experiments), virtually blocked by administration of the mix of voltage operate calcium channel (VOCC) blockers (two experiments). All traces represent the average of the kinetic analysis of all neurons present in a single imaged field (n = 5–10). (C) The spontaneous influx of Fe^{2+} was potentiated by further administration of either 30 mM KCl (in nine out of 15 experiments) or 100 μM NMDA (in seven out of 13 experiments). Both traces represent the average of six neurons. (D) Stimulation with 100 μM NMDA potentiated Fe^{2+} entry even in the presence of the mix of VOCC blockers, and this effect was partially inhibited by restoring 2 mM $[Ca^{2+}]_e$. The trace is the mean of seven neurons in the same experiment, representative of four independent experiments.

for the same entry pathways. These findings also provide evidence for a direct involvement of NMDARs in iron influx since quenching was observed even after VOCC blockade (Fig. 3D).

It should be finally pointed out that Fe^{2+} cannot simply substitute Ca^{2+} in channel permeation since activation of P_{2X} ionotropic receptors, present in neurons and permeable to Ca^{2+}, did not affect Fe^{2+} influx (see Fig. S1). This result also indicates that the transient $[Ca^{2+}]_i$ elevation elicited by ATP stimulation does not influence Fe^{2+} influx.

Iron-mediated ROS production and cell death

In the previous set of experiments we showed that an increase in extracellular Fe^{2+} promotes, *per se*, an influx of Fe^{2+} into the neurons and that either NMDAR stimulation or VOCC opening positively modulate this event. Based on these results, we decided to investigate the production of radicals as the primary effect of the intracellular accumulation of Fe^{2+}. ROS elevation was monitored, at the single cell level, by CM-H_2DCFDA, a reduced derivative of fluorescein, whose oxidation by ROS induces fluorescence increase. Measurements were performed with a high throughput microscopy (HTM) approach (IN Cell Analyzer 1000; GE Healthcare, Grandview Blvd, Waukesha, WI, USA), 30 min after various treatments and compared to untreated samples. The analysis was performed on neurons maintained in culture for either 9 or 15 days. Fe^{2+} promoted a significant ROS accumulation that was markedly potentiated by either depolarization or NMDA treatment. Noticeably, the elderly neurons showed significantly higher ROS production, when compared to the younger counterparts, only in the presence of Fe^{2+} (Fig. 4B). It should be noted that, in the absence of Fe^{2+} administration, the depolarization was ineffective, while NMDAR stimulation promoted ROS production (although the increase was not statistically significant), most likely by an alternative pathway (Fig. 4A). In line with these results, blockade of VOCCs in elderly neurons greatly reduced the ROS production induced by Fe^{2+} under depolarizing conditions and, to a lesser extent, also in non-stimulated conditions; moreover, under NMDA stimulation, the mix of VOCC blockers promoted a reduction comparable to unstimulated conditions (Fig. 4C). Based on morphologic features identified by the software of the IN Cell Analyzer 1000, ROS accumulation was mainly ascribable to neurons. To confirm this indication, we performed the same experiments on pure hippocampal astrocytes. ROS production did not increase upon Fe^{2+} administration, neither alone nor in the presence of KCl (data not shown), thereby indicating neurons as the main responsible for ROS accumulation.

We next investigated the effects of iron on neuronal viability. Cells were exposed to the above treatments for 60 min, stained with the death indicator Sytox orange and analyzed by HTM. Unfortunately, despite the possibility to investigate a large number of neurons, statistics were largely affected by the variable loss of dying cells during the washing steps (Semenova *et al.*, 2007). Nevertheless, the general trend observed in ROS measurements was clearly reproduced, with neuronal death significantly increased after exposure to the above protocols of stimulation (Fig. 5A). Once more, NMDA toxicity appears to involve pathways independent of Fe^{2+} entry. The cytotoxic

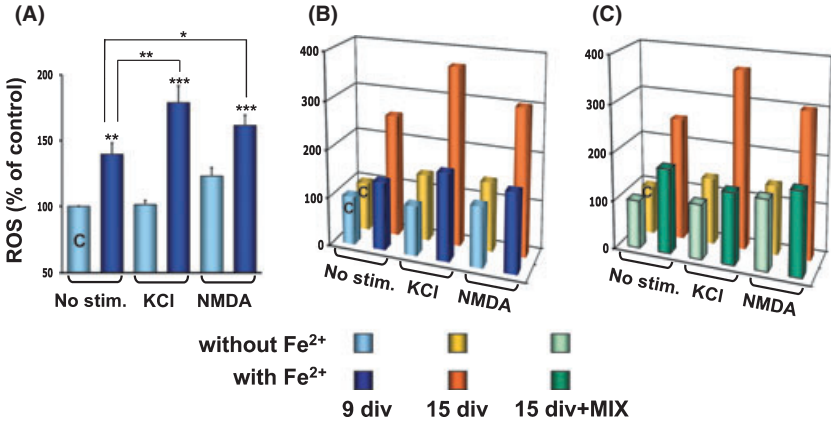

Fig. 4 Fe^{2+}-induced reactive oxygen species (ROS) production. (A) Hippocampal cultures grown for 9 days *in vitro* (either in the absence or in the presence of 100 μM Fe^{2+}) were exposed for 30 min to the following conditions: no stimulation; 30 mM KCl or 20 μM N-methyl-D-aspartic acid (NMDA). Afterward, cells were loaded with CM-H_2DCFDA and analyzed by high throughput microscopy for ROS production (see Experimental procedures). Data were recorded from 12 independent experiments in duplicate (~1000 cells per condition). In this, as well as in the other panels, the bars represent the mean (± SEM) of the fluorescent signals shown as percent of the control values (bars marked with C). (B) The results in A (bars with the same color) were compared with those obtained from older hippocampal cultures (15 days *in vitro*). With the time in culture, ROS production was significantly increased only in the presence of Fe^{2+}, in both unstimulated and stimulated conditions. (C) Results from 15 days-old cultures in B, were compared with data obtained from the same cultures (wells from the same plate) pretreated with a mix of VOOC blockers (10 μM nimodipine, 10 μM NNC 55-0396 and 1 μM ω-conotoxin MVIIC). In all Fe^{2+}-treated samples, the mix significantly reduced ROS production, although the effect was more marked under depolarizing condition, when voltage operate calcium channel opening directly potentiated Fe^{2+} entry (six experiments in duplicate, ~1000 cells per condition). Statistical significance in panel A was tested using one-way ANOVA followed by Bonferroni *post hoc* test. $*P < 0.05$; $**P < 0.01$; $***P < 0.001$. In panel B, ROS increase in older vs younger neurons was tested using two-way ANOVA, $P < 0.0001$. In panel C, the mix effects were tested using two-way ANOVA, $**P < 0.001$.

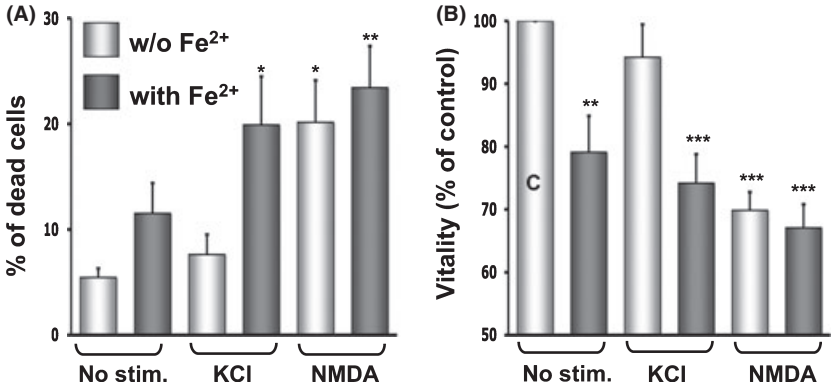

Fig. 5 Fe^{2+}-induced neuronal death. (A) Neuronal cells were treated for 60 min with the indicated stimuli before being stained with Sytox Orange. Fe^{2+}-induced cell death was evaluated by high throughput microscopy approach, as the percentage of Sytox Orange positive cells on the total number of neurons (approximately 400 neurons per well, in duplicate, 10 experiments). (B) Neuronal viability was evaluated by MTT assay, under the same experimental condition of A, as percent reduction with respect to control values (three experiments). Statistical significance was tested using one-way ANOVA followed by Bonferroni *post hoc* test. $*P < 0.05$; $**P < 0.01$; $***P < 0.001$.

effects of Fe^{2+} were fully confirmed by further analysis with MTT, a tetrazolium vital dye (Fig. 5B). With this assay, Fe^{2+} treatments showed statistically significant toxic effects, including simple Fe^{2+} administration. No changes in viability were observed in pure astrocyte cultures similarly processed in parallel (~5% cell death was measured in all experimental conditions).

Iron-dependent neuronal toxicity

In light of the evident role played by iron on neuronal viability, we investigated the mechanisms and the intracellular targets involved in iron-mediated neurotoxicity. In the following line of experiments we used 20 μM pyrithione, an iron ionophore (Kress *et al.*, 2002), to induce a faster iron entry and a controlled increase in its free cytosolic concentration (acute iron overload protocol, see Experimental procedures). Under this condition, single cell video-microscopy revealed a fast fura-2 fluorescence quenching (Fig. 6A). In all neurons, after the quenching caused by Fe^{2+} entry, a recovery of fluorescence was observed, variable in kinetics: delayed and extremely rapid in some cases, slowly progressing in others (red line in Fig. 6A and B, respectively). This dequenching was due to the oxidation of Fe^{2+} to Fe^{3+}, that was most likely induced by the Fenton reaction (see Fig. 7C), and that could be reproduced by adding H_2O_2 (see Fig. 1A). A parallel increase in ROS production was observed during this phase (by loading cells with both fura-2 and CM-H_2DCFDA), especially when glutathione (GSH) was previously depleted by L-buthionine sulfoximine (BSO) (not shown). ROS production (in particular hydroxyl radicals, highly toxic reactive species) can cause cytotoxic effects, eventually leading to neuron death. Indeed, the dequenching phase was promptly followed by an increase in $[Ca^{2+}]_i$ (343/380 ratio) most likely due to an aspecific influx. Shortly after, a sudden increase in the noise of 343/380 ratio and a drop in 355 nm signal clearly indicated the loss of fura-2 as a consequence of an increase in plasmalemma permeability also documented by Sytox blue nuclear staining (Fig. 6A,

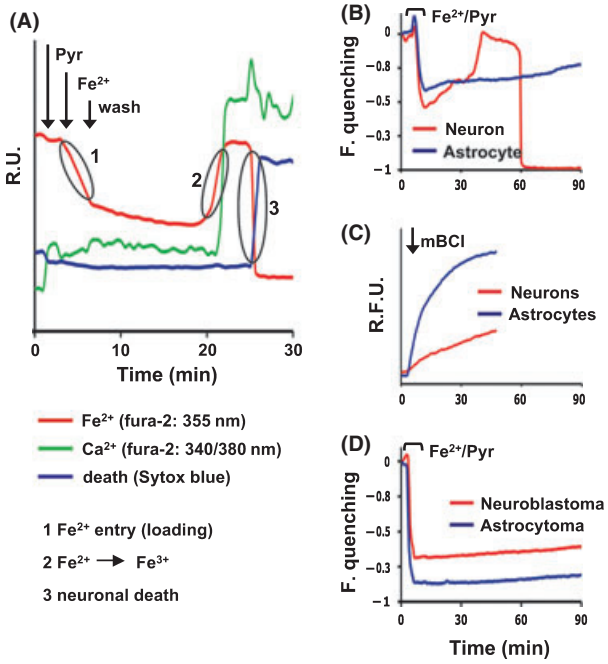

Fig. 6 Effects of acute Fe^{2+} overload. (A) Acute Fe^{2+} overload was performed by adding 20 μM pyrithione (Pyr, an iron ionophore) 2 min before administration of 1 μM Fe^{2+}. After 3 min, the excess of extracellular Fe^{2+} was washed out and cells were analyzed for up to 90 min. The traces represent different parameters analyzed within a single representative neuron (expressed as relative units, RU). (B) Upon acute Fe^{2+} overload (protocol as in A), astrocytes showed evidence of neither Fe^{2+} oxidation nor cell death when compared to the neurons present within the same field. Traces show changes in fura-2 fluorescence in two representative cells. (C) Hippocampal cultures were loaded with 50 μM mBCl, a probe that turns fluorescent after conjugation with glutathione (GSH). The difference in fluorescence plateau values (averaged in three neurons and three astrocytes within the same field) indicates a GSH content higher in astrocytes than in neuronal cells. R.F.U., relative fluorescence units. (D) Astrocytoma (U373) and neuroblastoma (Be2m17) cell lines subjected to acute Fe^{2+} overload (with 100 μM Fe^{2+}), did not show the typical toxic effects seen in neurons. Each trace (average of 40 cells) shows changes in fura-2 fluorescence.

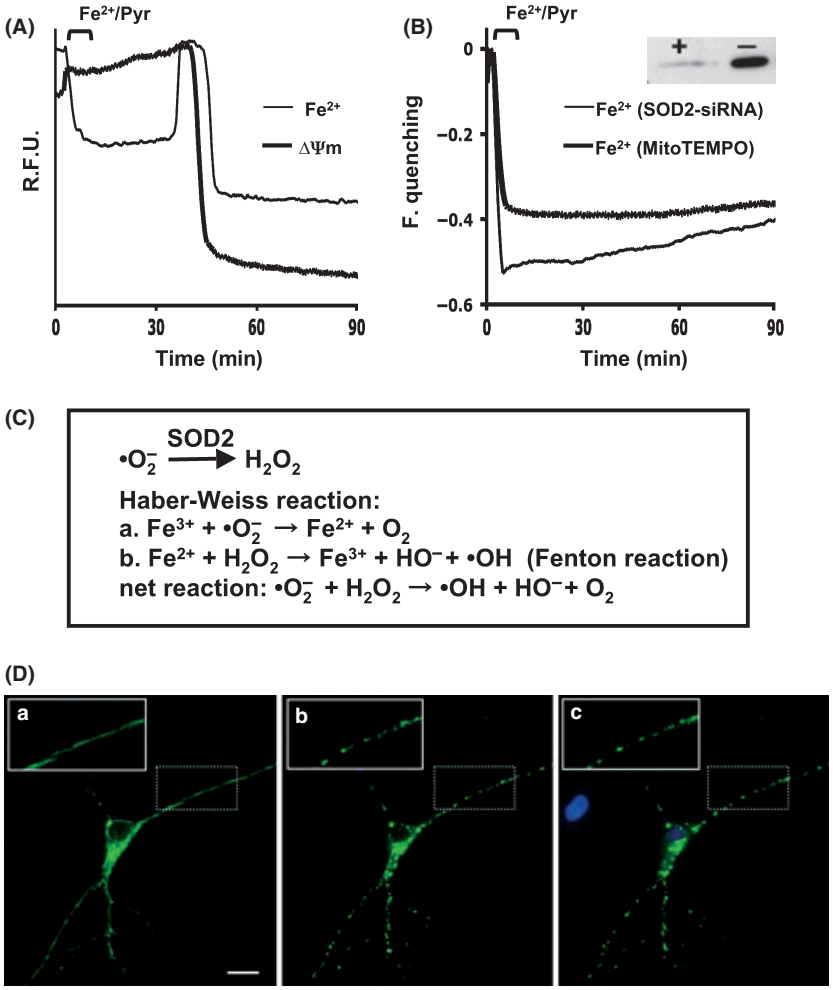

Fig. 7 Role of mitochondria in Fe^{2+}-induced neurotoxicity. (A) Neurons were loaded with both fura-2 and TMRM to monitor Fe^{2+} variations and mitochondrial membrane potential, respectively. The protocol of acute Fe^{2+} overload promoted neuronal death (loss of fura-2 signal), which was preceded by a drop in mitochondrial membrane potential. (B) Neurons either pre-treated for 60 min with 100 μM Mito-TEMPO (a mitochondrial superoxide scavenger) or previously transfected (48 h) with SOD2-siRNA, were protected from the typical Fe^{2+}-mediated toxic effects. The inset shows the western blot of SOD2 expression upon transfection with control (-) or SOD2-siRNA (+). (C) Schematic representation of reactions involved in neurotoxicity. SOD2 catalyzes $•O_2^-$ dismutation increasing H_2O_2 levels. The Fenton reaction shows that an increase in either Fe^{2+} or H_2O_2 levels favor the formation of highly toxic •OH. (D) Hippocampal neuron transfected with mitochondrial-targeted EYFP, were subjected to the protocol of acute iron overload and analyzed in the presence of 5 μM Sytox blue (a cell death indicator). Images were collected immediately after iron overload (a) and 40 (b) and 80 (c) min later. Mitochondrial fragmentation is highlighted in the insets of panel b and c. Scale bar: 25 μm.

see also the Movie S1). It must be pointed out that alterations in membrane integrity and cell death were not a consequence of the robust Ca^{2+} entry, since administration of excess EGTA in the extracellular solution did not prevent loss of fura-2 and Sytox staining (not shown). Compared to neurons, astrocytes showed very slow dequenching and no sign of membrane alterations, thus appearing more resistant to iron toxicity (Fig. 6B). Of note, after GSH depletion, astrocytes became as sensitive as neurons to iron toxicity (not shown). Therefore, susceptibility to iron load might be ascribed, at least partially, to the availability of reduced GSH. To test this hypothesis we compared the GSH levels in the two cell types. Hippocampal co-cultures were loaded with monochlorobimane (mBCl), a probe that turns fluorescent after conjugation with GSH. This method, based on an enzymatic reaction, offers the unique opportunity to evaluate GSH levels in neurons and astrocytes within co-cultures (Keelan *et al.*, 2001). The kinetics of fluorescent mBCl conjugate formation was followed for 30–40 min. In the hippocampal co-cultures, the fluorescence signal was very low in neurons and consistently higher in astrocytes (Fig. 6C), indicating a remarkable difference in GSH content as previously observed by Keelan and colleagues. The effects mediated by Fe^{2+} were investigated also in two neuroblastoma (SH-SY5Y and Be2m17) and in an astrocytoma (U373) exposed to the same protocol of acute iron-overload. In all cell lines the fluorescence quenching was stable for over 90 min, indicating a higher capability to prevent Fenton reaction and/or detoxify ROS, even in the presence of Fe^{2+} concentration up to 100 μM (Fig. 6D).

To characterize the mechanisms underlying iron-mediated neuronal toxicity, we analyzed the possible involvement of mitochondria, the main cellular sites of ROS production (Fariss *et al.*, 2005). To this purpose, cells were exposed to acute iron overload after loading with fura-2 and TMRM, a probe for mitochondrial membrane potential. Iron-induced cell death, monitored by fura-2 leakage, was preceded by complete loss of TMRM fluorescence, a sign of the collapse of mitochondrial membrane potential (Fig. 7A). The same results were obtained with JC-1, a similarly acting probe (data not shown). In light of these findings, cells were pre-incubated for 1 h with 100 μM Mito-TEMPO, a mitochondrial superoxide scavenger, before iron overload. Mito-TEMPO preserved mitochondrial membrane potential (data not shown) and protected hippocampal neurons against iron-induced neuronal injury (Fig. 7B) even when GSH had been previously depleted; on the contrary, Tempol, a cytosolic

scavenger, slowed down the cell death, but did not show a protective effect (not shown). Overall, this finding strongly indicates mitochondria as the main cellular target in iron-induced neuronal damage. As a next step, we investigated whether iron-induced mitochondrial alterations were caused by the anion superoxide itself, or were the consequence of its dismutation to H_2O_2 catalyzed by superoxide dismutase 2 (SOD2, see Fig. 7C). When specific small interfering RNAs silenced the SOD2 (verified by western blot analysis), neurons turned out to be protected, as in the experiments with mito-TEMPO (Fig. 7B), thereby suggesting that the reduction of mitochondrial level of H_2O_2 is crucial to prevent iron-mediated neuronal toxicity. Further evidence on the role of mitochondria is shown in Fig. 7D where cell death was preceded by fragmentation of these organelles.

Based on these premises, we investigated the protective effect of mito-TEMPO on the neuronal toxicity mediated by Fe^{2+} entry through Ca^{2+}-permeable channels, i.e. in the absence of the Fe^{2+} ionophore. A reduction in both ROS production and neuronal death was observed even after exposure to depolarizing conditions (Fig. 8). As expected from our previous findings, Mito-TEMPO was not able to exert a protective effect on NMDA-stimulated neurons, thereby confirming the presence of other neurotoxic pathways.

Discussion

Non-transferrin-bound iron is suggested to be mainly constituted by Fe^{2+}, because of the high concentration of ascorbate and the very low level of ferroxidase activity (mainly ceruplasmin) in the cerebrospinal fluid (Bradbury, 1997; Lane *et al.*, 2010). In the majority of this work, rat hippocampal primary cultures were challenged with high concentration of Fe^{2+} (up to 100 μM), to make the dynamics of fluorescence variations more evident and thus the analysis more reliable. Although this concentration is not necessarily unrealistic, since after hemorrhagic stroke a large amount of Fe^{2+} is released by dying erythrocytes (Wu *et al.*, 2003; Gaasch *et al.*, 2007b), we provide evidence that also concentrations of Fe^{2+} as low as 1 μM (concentrations measured in the cerebrospinal fluid; see Molina *et al.*, 1998; Bradbury, 1997) are effective in promoting intracellular iron load. Overall, we show that an increase in extracellular Fe^{2+} promotes a proportional Fe^{2+} entry in primary neuronal cells and that stimuli able to mimic pathways of synaptic activity, such as NMDAR activation and depolarization, positively modulate this event. Our data extend previous results obtained in cardiomyocytes and neuronal cell lines (NGF-differentiated PC12 cells and Neuro2A) in which L-type VOCCs were reported to be a direct route for Fe^{2+} uptake (Oudit *et al.*, 2003; Gaasch *et al.*, 2007a). In fact, our pharmacologic characterization indicates that not only L-type, but also other types of VOCCs are potentially involved in Fe^{2+} influx. Moreover, we showed that this pathway is mainly responsible for iron entry in resting neurons. Also the activation of NMDARs was reported in the literature to favor Fe^{2+} entry, however, via an indirect mechanism. According to the model proposed by Snyder's group (Cheah *et al.*, 2006),

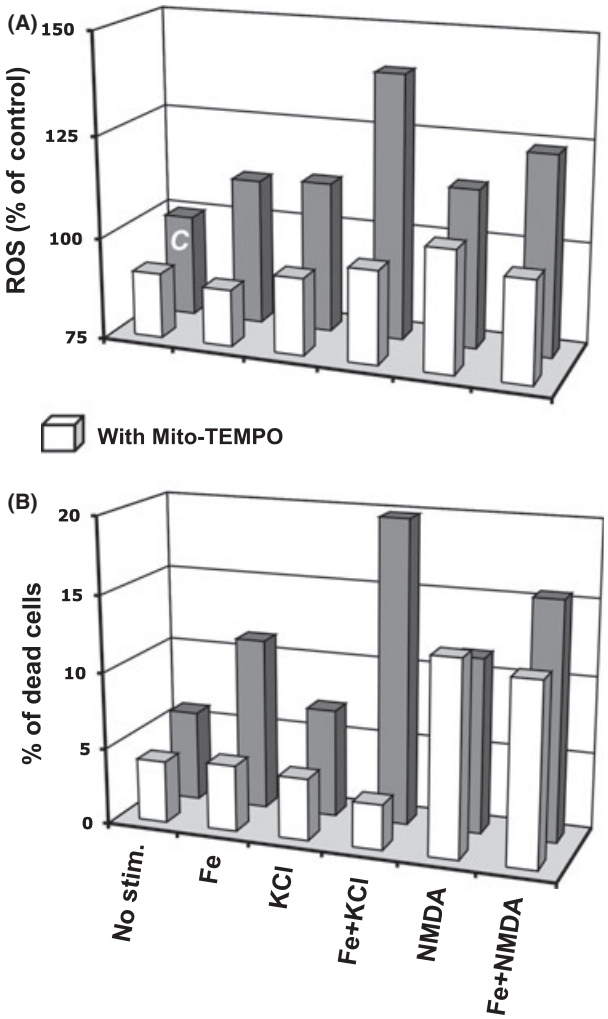

Fig. 8 Mitochondrial reactive oxygen species (ROS) scavenging protects against iron-induced neurotoxicity. Sixty minutes pre-treatment with 100 μM Mito-TEMPO reduced ROS formation (measured 30 min after stimulation, panel A) as well as the number of dead cells (analyzed 60 min after stimulation, panel B). The indicated experimental conditions apply to both panel A and B. Statistical significance of the difference between treatments performed in the absence or presence of Mito-TEMPO was tested using two-way ANOVA (five experiments, ~500 cells per well, in duplicate); (A) $P < 0.0001$, (B) $P < 0.01$.

NMDA-mediated Ca^{2+} influx is the key event triggering Fe^{2+} entry through a cascade of signals leading to a positive modulation of DMT1. Their model obviously implies that this Fe^{2+} transporter, which is known to be essential for intestinal iron absorption and for endosome-to-cytosol export of Tf-imported iron (Gunshin *et al.*, 1997; Andrews, 1999), is expressed in neuronal cells at the plasma membrane level. The experimental evidence we obtained in rat hippocampal neurons clearly argues against this proposal. First, our data show that not only VOCCs but also NMDARs promote potentiation of Fe^{2+} entry even in the absence of extracellular Ca^{2+} and thus in the absence of $[Ca^{2+}]_i$ elevation. Secondly, the competition between Fe^{2+} and Ca^{2+} entry in neurons represents a strong evidence that Fe^{2+} can flow directly through VOCCs and NMDARs. Finally, data in

the literature about the localization of DMT1 are somewhat controversial (Roth *et al.*, 2000; Lis *et al.*, 2004). We have recently addressed this issue in hippocampal neurons. Our data indicate that the DMT1 expression is low and mainly confined to cytoplasmic compartment; moreover, Total Internal Reflection Microscopy did not reveal GFP-DMT1 redistribution when neurons were bathed in Fe^{2+}-containing buffer (I. Pelizzoni, in preparation). We cannot exclude an involvement of DMT1 in other neuronal models (such as the neurons from cortex, analyzed in the study of Snyder's group) or in some pathologic conditions. Indeed, it was reported that the iron increase observed in Parkinson's disease might be sustained by changes in DMT1 levels (Chang *et al.*, 2006; Song *et al.*, 2007; Salazar *et al.*, 2008; Du *et al.*, 2009). Further investigation on the expression, regulation, and role of DMT1 in neurons from animal models in which the iron transport capacity of DMT1 is severely impaired (Belgrade rats or microcytic mice; Fleming *et al.*, 1997; Su *et al.*, 1998; Garrick *et al.*, 1999) might clarify this issue.

On the whole, it is clear that synaptic activity greatly enhances the possibility for iron to enter neurons also favoring cytotoxic effects. Of note, transient elevations of $[Ca^{2+}]_i$, either occurring as a consequence of the synaptic activity or evoked experimentally (e.g. by ATP stimulation), did not influence, *per se*, Fe^{2+} influx, at least within our experimental time window. Obviously, a modulation of Ca^{2+}-permeable channel activity can be promoted by sustained increase in $[Ca^{2+}]_i$. On the other hand, a Ca^{2+}-dependent transcriptional regulation of the expressions of the molecules involved in these iron entry pathways can occur at later times. Similarly, the elevation of intracellular iron can affect the expression of various proteins involved in iron homeostasis and, in particular, in iron influx, as it is the case for TfR and, possibly, for DMT1 (Hentze *et al.*, 2004; Galy *et al.*, 2008). Interestingly, our results suggest that Fe^{2+} ingress can be very harmful for cells since it depends on proteins (VOCCs and NMDARs) whose expression and activity are not controlled by iron overload.

In our conditions, at least a quote of the Fe^{2+} acquired by neurons is expected to accumulate in mitochondria, since iron-induced neuronal death was preceded by the change in the mitochondria morphology, from a continuous to a fragmented profile, and by the loss of the mitochondrial membrane potential, most likely caused by ROS increase. Indeed, treatment with a mitochondria-targeted superoxide anion scavenger (Mito-TEMPO) was able to reduce ROS accumulation, thereby preventing mitochondria disruption and consequent cell death. Similar treatments with cytosolic scavengers (such as Tempol) or antioxidant molecules (such as Trolox and N-acetyl cysteine) were not equally effective (I. Pelizzoni, unpublished data). According to the Fenton reaction (see Fig. 6C), iron toxicity largely depends on the levels of H_2O_2. Indeed, reduction of mitochondrial level of H_2O_2 by scavenging the superoxide anion or silencing SOD2 prevented iron-mediated neuronal toxicity. This result is in line with many studies indicating, rather surprisingly, that high levels of SOD may have detrimental effects on lifespan, most likely because the increase in superoxide dismutation leads to an elevation of H_2O_2 concentration (Giorgio *et al.*, 2007; Galaris *et al.*, 2008). This chain of events may be particularly dangerous during aging, when mitochondrial iron is reported to increase (Seo *et al.*, 2008; Ma *et al.*, 2009). Based on the above considerations, it will be crucial to investigate the mechanisms underlying iron import and handling into mitochondria, two aspects still largely obscure, especially at the neuronal level. It should be finally observed that in the presence of NMDA stimulation, Mito-TEMPO prevented ROS formation, but not neuronal death. This behavior can be ascribed to the complexity of the NMDA-mediated excitotoxic process in which, a deregulation of cytosolic Ca^{2+} and a drop in mitochondrial ATP production represent the main causes of neuronal death (Atlante *et al.*, 2001; Nicholls *et al.*, 2007). Our data support the idea that dysregulation of the two ions involves distinct metabolic pathways that, however, can converge (Robb *et al.*, 1999; Nicholls *et al.*, 2007). A complex interplay between calcium and iron in neuronal homeostasis as well as in neurodegenerative processes can thus be envisaged (Pelizzoni *et al.*, 2008).

A final comment should be made on the responsiveness of different kinds of cells to iron. Neuronal cells appeared more vulnerable to iron overload and more prone to death than astrocytes (see also Kress *et al.*, 2002). Interestingly, the cellular susceptibility to iron appears to correlate with the level of 'labile iron pool' (LIP; see Breuer *et al.*, 1996, for a definition): virtually undetectable in primary neurons, barely measurable in astrocytes, while clearly assessable in neuronal cell lines (e.g. SH-SY5Y; data not shown). This finding suggests that neuronal cells must exert a tight control of intracellular free iron to avoid the ensuing toxic effects. Astrocytes, although more resistant than neurons to oxidative stress, are also vulnerable to iron-induced toxicity depending on the culture conditions. It remains to be established whether astrocyte detoxifying properties can contribute to neuron protection. Finally, it is important to stress that brain-derived cell lines (both neuroblastoma and astrocytoma) consistently showed higher resistance to iron toxicity than their primary cell counterparts.

In conclusion, although neurons take up iron mainly through the TfR-route, other pathways play an important role, particularly in the presence of NTBI elevation. These pathways can have an important physiologic relevance but appear critical in pathologic conditions of iron accumulation since they are not controlled by feedback mechanisms. In this scenario, along with pharmacologic approaches aimed to reduce oxidative stress, harnessing iron entry through Ca^{2+}-permeable channels might contribute to control neurodegenerative processes due to physiologic aging or promoted by pathologic alterations of iron handling.

Experimental procedures

Cell cultures

Primary cultures of hippocampal neurons were prepared according to Codazzi *et al.* (2006) from 2 to 3 day-old Sprague–Dawley rats. The Institutional Animal Care and Use Committee of the S. Raffaele Scientific Institute approved the experimental

procedures. Briefly, after quick subdivision of hippocampi into small sections, the tissue was incubated into Hank's solution containing 3.5 mg mL^{-1} trypsin type IX (Sigma-Aldrich, St Louis, MO, USA) and 0.5 mg mL^{-1} DNase type IV (Calbiochem, La Jolla, CA, USA) for 5 min. The pieces were then mechanically dissociated in a Hank's solution supplemented with 12 mM $MgSO_4$ and 0.5 mg mL^{-1} DNase IV. After centrifugation, cells were plated onto poly-ornithine coated coverslips and maintained in MEM supplemented with 0.6% glucose, B27, 2 mM glutamax, 5% fetal calf serum and 3 μM 1-β-D-cytosine-arabinofuranoside (Ara-C; Sigma-Aldrich). Cultures were maintained at 37°C in a 5% CO_2 humidified incubator, and used up to 15 days after plating.

Primary cultures of hippocampal pure astrocytes were dissociated according to the same protocol as above. Astrocytes were grown in MEM supplemented with 10% horse serum (PAA Laboratories, Laboratories GmbH, Pasching, Austria), 33 mM glucose, 2 mM glutamax and 50 U mL^{-1} Pen/Strep. Two steps of overnight shaking at 230 rpm were performed to induce selective detachment of microglia. After reaching confluence, astrocytes were trypsinized and re-plated onto poly-lysine-coated plastic multiwells. Experiments were performed within 3 days after re-plating. When not specified, chemicals were from Gibco BRL (Invitrogen, Carlsbad, CA, USA).

Videomicroscopy setup

The videoimaging setup is based on an Axioskope 2 microscope (Zeiss, Oberkochen, Germany) and a Polychrome IV (Till Photonics, GmbH, Martinsried, Germany) light source. Fura-2 was excited at 340 and 380 nm for Ca^{2+} measurements and at 355 nm to monitor Fe^{2+} variations (as quenching of the fluorescence signal). The excitation wavelength of 355 nm was adopted as it turned out to be insensitive to Ca^{2+} variations in our optical configuration. Fluorescence images were collected by a cooled CCD videocamera (PCO Computer Optics GmbH, Kelheim, Germany). The 'Vision' software (Till Photonics) was used to control the acquisition protocol and to perform data analysis. The IN Cell Analyzer 1000 (GE Healthcare) was used for HTM.

Solutions and dye loading

Dye loading and single cell experiments were performed in Krebs Ringer Hepes buffer (KRH, containing 5 mM KCl, 125 mM NaCl, 2 mM $CaCl_2$, 1.2 mM $MgSO_4$, 1.2 mM KH_2PO_4 and 6 mM glucose, 20 mM Hepes, pH 7.4). When K^+ concentration was increased in the solution, the concentration of Na^+ was adjusted to maintain isotonicity. To obtain Ca^{2+}/Mg^{2+}-free KRH, a modified KRH solution without added divalent ions was incubated on a rotating wheel with CHELEX-100 resin (Sigma-Aldrich; 2.5 g for 50 mL of KRH, at 4°C for 48 h) to eliminate the traces of Ca^{2+} and Mg^{2+}. Afterward, the solution was pH checked. Experiments were performed at room temperature.

The fluorescent dyes (from Molecular Probes, Invitrogen, Carlsbad, CA, USA, when not specified) were administered as follows: (i) fura-2 acetoxymethyl ester (Calbiochem): 40 min at 37°C, 4 μM final concentration; (ii) 5-(and-6)-chloromethyl-2′,7′-dichlorodihydrofluorescein diacetate, acetyl ester (CM-H_2DCFDA): 30 min at 37°C, 0.25 μM final concentration; (iii) Sytox orange: 5 min at room temperature, 5 μM final concentration; (iv) Sytox blue: kept in the bath during the experiments, 5 μM final concentration; (v) Hoechst: 5 min at room temperature, 10 μg mL^{-1} final concentration; (vi) Tetramethyl rhodamine methyl ester (TMRM): 15 min at room temperature (and maintained in the bath during the experiment), 25 nM final concentration; (vii) calcein acetoxymethyl ester: 3 min at 37°C, 0.25 μM final concentration. If not otherwise specified, after dye loading, cells were washed twice with fresh KRH and kept in the same buffer.

Cellular treatments

Fe^{2+} was freshly prepared as a solution of ferrous-ammonium sulfate (kept in ice until use). The acute iron overload protocol was: incubation of cells in the presence of 20 μM pyrithione, an iron ionophore, for 2 min; administration of Fe^{2+} to the desired concentration for 3 min; several washes with KRH.

In some experiments cells were pre-treated with drugs or pharmacologic agents as follows: (i) 100 μM (2-(2,2,6,6-Tetramethylpiperidin-1-oxyl-4-ylamino)-2-oxoethyl) triphenylphosphonium chloride monohydrate (Mito-TEMPO; Alexis Biochemicals, Lausen, Switzerland) was added to cells 1 h before the experiment and kept in the extracellular buffer during the experiment; (ii) the NMDAR antagonist MK-801 (20 μM) and the mix of VOCC blockers (10 μM nimodipine, Sigma-Aldrich; 1 μM ω-conotoxin-MVIIC, Tocris, Bristol, UK; 10 μM NNC 55-0396, Tocris) were administered 15 min before the beginning of the experiment and kept in the extracellular solution until the end; (iii) 500 μM BSO (Sigma-Aldrich), an inhibitor of GSH synthesis, was added 24 h before the experiment.

Measurements of ROS, cell death, and cell viability

Cells were washed with KRH and then exposed to different experimental protocols for 30 (ROS) or 60 (cell death) min. After washing, the cells were loaded with Hoechst, a cell-permeant nuclear dye and with either CM-H_2DCFDA (ROS indicator) or Sytox orange (cell death probe). The cells were then studied by the IN Cell Analyzer 1000.

Cell viability was quantified by 3-(4,5-Dimethylthiazol-2-yl)-2,5-diphenyltetrazolium bromide (MTT) assay. Briefly, primary co-cultures were plated on 96-wells or 24-wells plates and maintained in culture for at least 12 days. Afterward, cells were washed once with KRH buffer and exposed to the experimental protocols for 1 h at 37°C. After washing, cells were incubated for 1 h with 0.5 mg mL^{-1} MTT (Sigma-Aldrich) in either KRH or conditioned medium. After removing the extracellular solution, formazan, the MTT metabolic product, was dissolved in DMSO and the absorbance was read at 570 nm.

Data analysis

Data are presented as mean ± SEM as specified. Statistical significance was tested using two-way ANOVA or one-way ANOVA followed by Dunnett's (for multiple comparisons against a single reference group) or Bonferroni (for all pair wise comparisons) *post hoc* tests. Statistical analysis was performed using GraphPad Prism (GraphPad Software, San Diego, CA, USA).

Acknowledgments

We thank all the people of NFC Unit at S. Raffaele Institute for helpful discussion and support, R. Fesce for statistical analysis, B. Rossetti for revision of the manuscript. Financial support was from the Italian Ministry of Research (PRIN, Progetti di Ricerca di Interesse Nazionale, project 2006054051 to F.G.) and the Italian Telethon Foundation (GGP05141 and GGP00099 grants to F.G.).

References

Altamura S, Muckenthaler MU (2009) Iron toxicity in diseases of aging: Alzheimer's disease, parkinson's disease and atherosclerosis. *J. Alzheimers Dis.* **16**, 879–895.

Andersen JK (2004) Oxidative stress in neurodegeneration: cause or consequence? *Nat. Med.* **10** (Suppl.), S18–S25.

Andrews NC (1999) The iron transporter DMT1. *Int. J. Biochem. Cell Biol.* **31**, 991–994.

Atlante A, Calissano P, Bobba A, Giannattasio S, Marra E, Passarella S (2001) Glutamate neurotoxicity, oxidative stress and mitochondria. *FEBS Lett.* **497**, 1–5.

Benarroch EE (2009) Brain iron homeostasis and neurodegenerative disease. *Neurology* **72**, 1436–1440.

Bradbury MW (1997) Transport of iron in the blood-brain-cerebrospinal fluid system. *J. Neurochem.* **69**, 443–454.

Bralet J, Schreiber L, Bouvier C (1992) Effect of acidosis and anoxia on iron delocalization from brain homogenates. *Biochem. Pharmacol.* **43**, 979–983.

Breuer W, Epsztejn S, Cabantchik ZI (1996) Dynamics of the cytosolic chelatable iron pool of K562 cells. *FEBS Lett.* **382**, 304–308.

Britigan BE, Rasmussen GT, Cox CD (1998) Binding of iron and inhibition of iron-dependent oxidative cell injury by the ''calcium chelator'' 1,2-bis(2-aminophenoxy)ethane N,N,N′,N′-tetraacetic acid (BAPTA). *Biochem. Pharmacol.* **55**, 287–295.

Cabantchik ZI, Glickstein H, Milgram P, Breuer W (1996) A fluorescence assay for assessing chelation of intracellular iron in a membrane model system and in mammalian cells. *Anal. Biochem.* **233**, 221–227.

Chang YZ, Ke Y, Du JR, Halpern GM, Ho KP, Zhu L, Gu XS, Xu YJ, Wang Q, Li LZ, Wang CY, Qian ZM (2006) Increased divalent metal transporter 1 expression might be associated with the neurotoxicity of L-DOPA. *Mol. Pharmacol.* **69**, 968–974.

Cheah JH, Kim SF, Hester LD, Clancy KW, Patterson SE 3rd, Papadopoulos V, Snyder SH (2006) NMDA receptor-nitric oxide transmission mediates neuronal iron homeostasis via the GTPase Dexras1. *Neuron* **51**, 431–440.

Codazzi F, Di Cesare A, Chiulli N, Albanese A, Meyer T, Zacchetti D, Grohovaz F (2006) Synergistic control of protein kinase cgamma activity by ionotropic and metabotropic glutamate receptor inputs in hippocampal neurons. *J. Neurosci.* **26**, 3404–3411.

Du F, Qian ZM, Zhu L, Wu XM, Yung WH, Tsim TY, Ke Y (2009) L-DOPA neurotoxicity is mediated by up-regulation of DMT1-IRE expression. *PLoS ONE* **4**, e4593.

Esposito BP, Epsztejn S, Breuer W, Cabantchik ZI (2002) A review of fluorescence methods for assessing labile iron in cells and biological fluids. *Anal. Biochem.* **304**, 1–18.

Fariss MW, Chan CB, Patel M, Van Houten B, Orrenius S (2005) Role of mitochondria in toxic oxidative stress. *Mol. Interv.* **5**, 94–111.

Fleming MD, Trenor CC 3rd, Su MA, Foernzler D, Beier DR, Dietrich WF, Andrews NC (1997) Microcytic anaemia mice have a mutation in Nramp2, a candidate iron transporter gene. *Nat. Genet.* **16**, 383–386.

Gaasch JA, Geldenhuys WJ, Lockman PR, Allen DD, Van der Schyf CJ (2007a) Voltage-gated calcium channels provide an alternate route for iron uptake in neuronal cell cultures. *Neurochem. Res.* **32**, 1686–1693.

Gaasch JA, Lockman PR, Geldenhuys WJ, Allen DD, Van der Schyf CJ (2007b) Brain iron toxicity: differential responses of astrocytes, neurons, and endothelial cells. *Neurochem. Res.* **32**, 1196–1208.

Galaris D, Mantzaris M, Amorgianiotis C (2008) Oxidative stress and aging: the potential role of iron. *Hormones* (Athens) **7**, 114–122.

Galy B, Ferring-Appel D, Kaden S, Gröne HJ, Hentze MW (2008) Iron regulatory proteins are essential for intestinal function and control key iron absorption molecules in the duodenum. *Cell Metab.* **7**, 79–85.

Garrick LM, Dolan KG, Romano MA, Garrick MD (1999) Non-transferrin-bound iron uptake in belgrade and normal rat erythroid cells. *J. Cell. Physiol.* **178**, 349–358.

Giorgio M, Trinei M, Migliaccio E, Pelicci PG (2007) Hydrogen peroxide: a metabolic by-product or a common mediator of ageing signals? *Nat. Rev. Mol. Cell Biol.* **8**, 722–728.

Gunshin H, Mackenzie B, Berger UV, Gunshin Y, Romero MF, Boron WF, Nussberger S, Gollan JL, Hediger MA (1997) Cloning and characterization of a mammalian proton-coupled metal-ion transporter. *Nature* **388**, 482–488.

Hentze MW, Muckenthaler MU, Andrews NC (2004) Balancing acts: molecular control of mammalian iron metabolism. *Cell* **117**, 285–297.

Keelan J, Allen NJ, Antcliffe D, Pal S, Duchen MR (2001) Quantitative imaging of glutathione in hippocampal neurons and glia in culture using monochlorobimane. *J. Neurosci. Res.* **66**, 873–884.

Kress GJ, Dineley KE, Reynolds IJ (2002) The relationship between intracellular free iron and cell injury in cultured neurons, astrocytes, and oligodendrocytes. *J. Neurosci.* **22**, 5848–5855.

Lane DJ, Robinson SR, Czerwinska H, Bishop GM, Lawen A (2010) Two routes of iron accumulation in astrocytes: ascorbate-dependent ferrous iron uptake via the divalent metal transporter (DMT1) plus an independent route for ferric iron. *Biochem. J.* **432**, 123–132.

Lipscomb DC, Gorman LG, Traystman RJ, Hurn PD (1998) Low molecular weight iron in cerebral ischemic acidosis *in vivo*. *Stroke* **29**, 487–493.

Lis A, Barone TA, Paradkar PN, Plunkett RJ, Roth JA (2004) Expression and localization of different forms of DMT1 in normal and tumor astroglial cells. *Brain Res. Mol. Brain Res.* **122**, 62–70.

Ma YS, Wu SB, Lee WY, Cheng JS, Wei YH (2009) Response to the increase of oxidative stress and mutation of mitochondrial DNA in aging. *Biochim. Biophys. Acta* **1790**, 1021–1029.

MacKenzie EL, Iwasaki K, Tsuji Y (2008) Intracellular iron transport and storage: from molecular mechanisms to health implications. *Antioxid. Redox Signal.* **10**, 997–1030.

Madsen E, Gitlin JD (2007) Copper and iron disorders of the brain. *Annu. Rev. Neurosci.* **30**, 317–337.

Mills E, Dong XP, Wang F, Xu H (2010) Mechanisms of brain iron transport: insight into neurodegeneration and CNS disorders. *Future Med. Chem.* **2**, 51.

Molina JA, Jimenez-Jimenez FJ, Aguilar MV, Meseguer I, Mateos-Vega CJ, Gonzalez-Munoz MJ, de Bustos F, Porta J, Orti-Pareja M, Zurdo M, Barrios E, Martinez-Para MC (1998) Cerebrospinal fluid levels of transition metals in patients with alzheimer's disease. *J. Neural Transm.* **105**, 479–488.

Moos T, Morgan EH (2004) The metabolism of neuronal iron and its pathogenic role in neurological disease. *Ann. N Y Acad. Sci.* **1012**, 14–26.

Moos T, Rosengren Nielsen T, Skjorringe T, Morgan EH (2007) Iron trafficking inside the brain. *J. Neurochem.* **103**, 1730–1740.

Nicholls DG, Johnson-Cadwell L, Vesce S, Jekabsons M, Yadava N (2007) Bioenergetics of mitochondria in cultured neurons and their role in glutamate excitotoxicity. *J. Neurosci. Res.* **85**, 3206–3212.

Oudit GY, Sun H, Trivieri MG, Koch SE, Dawood F, Ackerley C, Yazdanpanah M, Wilson GJ, Schwartz A, Liu PP, Backx PH (2003) L-type Ca^{2+} channels provide a major pathway for iron entry into cardiomyocytes in iron-overload cardiomyopathy. *Nat. Med.* **9**, 1187–1194.

Pelizzoni I, Macco R, Zacchetti D, Grohovaz F, Codazzi F (2008) Iron and calcium in the central nervous system: a close relationship in health and sickness. *Biochem. Soc. Trans.* **36**, 1309–1312.

Qian ZM, Shen X (2001) Brain iron transport and neurodegeneration. *Trends Mol. Med.* **7**, 103–108.

Robb SJ, Robb-Gaspers LD, Scaduto RC Jr, Thomas AP, Connor JR (1999) Influence of calcium and iron on cell death and mitochondrial function in oxidatively stressed astrocytes. *J. Neurosci. Res.* **55**, 674–686.

Roth JA, Horbinski C, Feng L, Dolan KG, Higgins D, Garrick MD (2000) Differential localization of divalent metal transporter 1 with and without iron response element in rat PC12 and sympathetic neuronal cells. *J. Neurosci.* **20**, 7595–7601.

Salazar J, Mena N, Hunot S, Prigent A, Alvarez-Fischer D, Arredondo M, Duyckaerts C, Sazdovitch V, Zhao L, Garrick LM, Nunez MT, Garrick MD, Raisman-Vozari R, Hirsch EC (2008) Divalent metal transporter 1 (DMT1) contributes to neurodegeneration in animal models of parkinson's disease. *Proc. Natl. Acad. Sci. USA* **105**, 18578–18583.

Semenova MM, Mäki-Hokkonen AM, Cao J, Komarovski V, Forsberg KM, Koistinaho M, Coffey ET, Courtney MJ (2007) Rho mediates calcium-dependent activation of p38alpha and subsequent excitotoxic cell death. *Nat. Neurosci.* **10**, 436–443.

Seo AY, Xu J, Servais S, Hofer T, Marzetti E, Wohlgemuth SE, Knutson MD, Chung HY, Leeuwenburgh C (2008) Mitochondrial iron accumulation with age and functional consequences. *Aging Cell* **7**, 706–716.

Shvartsman M, Kikkeri R, Shanzer A, Cabantchik ZI (2007) Non-transferrin-bound iron reaches mitochondria by a chelator-inaccessible mechanism: biological and clinical implications. *Am. J. Physiol. Cell Physiol.* **293**, C1383–C1394.

Song N, Jiang H, Wang J, Xie JX (2007) Divalent metal transporter 1 up-regulation is involved in the 6-hydroxydopamine-induced ferrous iron influx. *J. Neurosci. Res.* **85**, 3118–3126.

Stankiewicz JM, Brass SD (2009) Role of iron in neurotoxicity: a cause for concern in the elderly? *Curr. Opin. Clin. Nutr. Metab. Care* **12**, 22–29.

Su MA, Trenor CC, Fleming JC, Fleming MD, Andrews NC (1998) The G185R mutation disrupts function of the iron transporter Nramp2. *Blood* **92**, 2157–2163.

Vargas JD, Herpers B, McKie AT, Gledhill S, McDonnell J, van den Heuvel M, Davies KE, Ponting CP (2003) Stromal cell-derived receptor 2 and cytochrome b561 are functional ferric reductases. *Biochim. Biophys. Acta* **1651**, 116–123.

Wu J, Hua Y, Keep RF, Nakamura T, Hoff JT, Xi G (2003) Iron and iron-handling proteins in the brain after intracerebral hemorrhage. *Stroke* **34**, 2964–2969.

Wu LJ, Leenders AG, Cooperman S, Meyron-Holtz E, Smith S, Land W, Tsai RY, Berger UV, Sheng ZH, Rouault TA (2004) Expression of the iron transporter ferroportin in synaptic vesicles and the blood-brain barrier. *Brain Res.* **1001**, 108–117.

Zecca L, Youdim MB, Riederer P, Connor JR, Crichton RR (2004) Iron, brain ageing and neurodegenerative disorders. *Nat. Rev. Neurosci.* **5**, 863–873.

Supporting Information

Additional supporting information may be found in the online version of this article:

Fig. S1 Effect of ATP administration on Fe^{2+} influx.

Movie S1. Dynamics of acute iron overload effects.

As a service to our authors and readers, this journal provides supporting information supplied by the authors. Such materials are peer-reviewed and may be re-organized for online delivery, but are not copy-edited or typeset. Technical support issues arising from supporting information (other than missing files) should be addressed to the authors.